

Cover Page



Universiteit Leiden



The handle <http://hdl.handle.net/1887/36422> holds various files of this Leiden University dissertation.

**Author:** Díaz Morales, Oscar Alfonso

**Title:** Catalysis of the electrochemical water oxidation to oxygen

**Issue Date:** 2015-11-19

# Chapter 2

---

## **Evidences for gold oxide decomposition mechanism during the electrochemical water oxidation**

### **ABSTRACT**

In this chapter we study through a multiplicity of experimental and theoretical techniques the electrochemical evolution of oxygen on gold, the metal on which water splitting was initially discovered more than two centuries ago. The evidence obtained with a combination of *in situ* surface-enhanced Raman spectroscopy, online electrochemical mass spectrometry and density functional theory calculations suggests the existence of several mechanisms for the evolution of O<sub>2</sub> on Au electrodes, depending on the electrode potential. Significantly, at approximately 2.0 V vs. RHE the first O<sub>2</sub> that is evolved consists of two oxygens from the surface oxide, suggesting an oxide decomposition or oxide disproportionation step. At somewhat higher potentials, O<sub>2</sub> is formed by a combination of oxygen from the oxide lattice and oxygen provided by water. The oxide decomposition step implies a more three-dimensional mechanism for oxygen evolution than previously suggested mechanisms, which involve only surface-adsorbed intermediates.

---

This chapter has been published in: Diaz-Morales, O.; Calle-Vallejo, F.; de Munck, C. and Koper M.T.M. *Chemical Science* **2013**, 4, 2334-2343.

## 2.1. Introduction

The first recorded experiment on water electrolysis was carried out by Adriaan Paets van Troostwijk and Jan Rudolph Deiman in Haarlem, The Netherlands, in 1789.<sup>1,2</sup> Paets van Troostwijk and Deiman used an electrostatic machine invented by Martinus van Marum to discharge an electric potential difference between two gold electrodes in a Leyden jar filled with water. Hydrogen evolved on one gold electrode, and oxygen evolved on the other gold electrode.

Almost two hundred and twenty five years later, water splitting is considered as an important part of what many consider to be the only sustainable solution to the world's energy problem.<sup>3,4</sup> Using sunlight to generate photo-excited electrons and holes would allow the photo-electrocatalytic synthesis of hydrogen and oxygen. Hydrogen would be the fuel to store the sun's energy, and may be converted back into electricity in a fuel cell, using the reverse reaction to water electrolysis. It is generally recognized that one of the key fundamental bottlenecks in making the (photo-)electrochemical generation of fuels a viable technology lies in the poor kinetics of the anode reaction, *i.e.* the water oxidation to oxygen.

The best and most stable inorganic catalysts for water splitting are oxides.<sup>5,6</sup> In spite of decades of research into the oxygen-evolving activities of a large variety of oxides, the suggested mechanisms for oxide-catalyzed water splitting are surprisingly simple and “two-dimensional”, focused on reaction intermediates that exist directly at the oxide-electrolyte interface.<sup>5,7,8</sup> However, explicit spectroscopic evidence for such pathways is still largely missing. One possible exception is a recent study by Yeo et al.<sup>9</sup> who observed a vibrational signal near  $820\text{ cm}^{-1}$  using Surface-Enhanced Raman Spectroscopy (SERS) during the oxygen evolution on gold both in acid and alkaline media. They attributed this signal to the formation of a surface-bound hydroperoxy intermediate.

In this chapter, we return to the electrode material originally used by Paets van Troostwijk and Deiman, and discuss the possibility of a new mechanism for the oxygen

evolution on gold electrodes covered by a thin oxide, based on a combination of electrochemistry, *in situ* Surface-Enhanced Raman Spectroscopy, online electrochemical mass spectrometry (OLEMS), and first-principles density functional theory (DFT) calculations. Our model is significantly different from the models advocated in the literature and supported in the recent SERS work of Yeo et al. The key ingredient of our model is that we assume that the thin but distinctly three-dimensional nature of the gold oxide is intimately involved in the mechanism, and that oxygen is evolved not through the coupling of surface intermediates, but as the result of the decomposition of the unstable three-dimensional surface oxide releasing molecular oxygen into the solution. Such a new mechanism, if correct, could suggest novel strategies towards developing better inorganic water splitting catalysts.

## 2.2. Experimental and Computational Section

### 2.2.1. Experimental

All glassware was thoroughly cleaned before starting experiments by boiling in 1:10 mixture of 30% H<sub>2</sub>O<sub>2</sub> / concentrated H<sub>2</sub>SO<sub>4</sub> to remove organic contaminations, and was subsequently boiled five times in Millipore Milli-Q water (resistivity >18.2 MΩ cm). Electrolyte solutions were prepared with Suprapur (Merck) reagents and Milli-Q water. Dissolved oxygen in solutions was removed prior to measurements by purging with argon (purity grade 5.0) for at least 30 min, and the argon was kept flowing above solution during experiments. Experiments with <sup>18</sup>O enriched water were performed with 98% <sup>18</sup>O water (GMP standard, purchased from CMR).

*In situ* Surface Enhanced Raman Spectroscopy (SERS) was performed with a confocal Raman microscope (LabRam HR, Horiba Yobin Yvon) with a 50X objective. A He/Ne laser (633 nm) was used as excitation source. Backscattered light was filtered by a 633 nm edge filter, directed to the spectrograph and to the detector. Details of the setup can be found in reference 10. The electrochemical SERS experiments were made with an Ivium potentiostat/galvanostat (IviumStat), using a home-made electrochemical cell with a small

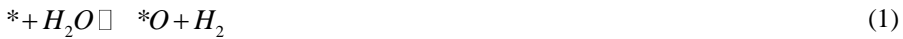
electrolyte volume necessary for the  $\text{H}_2^{18}\text{O}$  experiments. The electrochemical cell has one compartment and three electrodes, a gold wire as counter electrode, reversible hydrogen electrode (RHE) as reference electrode (all potentials in this work are reported versus this reference electrode unless otherwise stated) and a roughened gold surface as working electrode. The working electrode was mechanically polished to mirror finish using alumina with different grain sizes to  $0.3\ \mu\text{m}$ , rinsed with Milli-Q water and ultrasonicated during 15 min to remove all residuals of mechanical polishing. Next, the gold electrode was electrochemically roughened by 25 oxidation-reduction cycles (ORC) in  $0.1\ \text{M}\ \text{KCl}$ . The ORC were performed between  $-0.30$  and  $1.20\ \text{V}$  vs. SCE, during which the potential was held for 30 seconds at the negative limit and for 1.3 seconds at the positive limit, a method reported to give a brownish surface that is SERS active.<sup>11</sup>

Online Electrochemical Mass Spectrometry (OLEMS) experiments were performed using an EvoLution mass spectrometer system (European Spectrometry systems Ltd). The setup has a mass detector (Prisma QMS200, Pfeiffer) which was brought to vacuum using both a turbo molecular pump (TMH-071P, Pfeiffer, flow rate  $60\ \text{L}\ \text{s}^{-1}$ ) and a rotary vane pump (Duo 2.5, Pfeiffer; flow rate  $2.5\ \text{m}^3\ \text{h}^{-1}$ ). During measurements, the pressure inside the mass detector chamber was around  $10^{-6}$  mbar. Volatile reaction products were collected from electrode interface by a small inlet tip positioned close ( $\sim 10\ \mu\text{m}$ ) to electrode surface using a micrometric screw system and a camera.<sup>12</sup> The inlet tip is made with a porous Teflon cylinder (Porex®) mounted in a Kel-F holder. The inlet is connected to the mass detector through a PEEK capillary. Before use, the inlet tip was cleaned during 15 min with a solution  $0.2\ \text{M}\ \text{K}_2\text{Cr}_2\text{O}_7$  in  $2\ \text{M}\ \text{H}_2\text{SO}_4$  and rinsed thoroughly with Milli-Q water.

### 2.2.2. Computational

All adsorption energies were calculated by means of DFT simulations using the Vienna Ab-initio Simulation Package (VASP)<sup>13</sup>. The exchange and correlation parts of the total energies were estimated with the Perdew-Burke-Ernzerhof (PBE) functional.<sup>14</sup> The Au surfaces were represented by supercells in which the lattice constant was  $4.18\ \text{Å}$ , corresponding to an interatomic distance of  $2.95\ \text{Å}$ . Four atomic layers were used to

represent the surfaces, of which the topmost two and the adsorbates were fully allowed to relax whereas the bottom layers were fixed at the bulk equilibrium distances. The vertical separation between successive slabs was always more than 15 Å and dipole corrections were applied. In the search for optimal geometries the kinetic energy cut-off of the plane-wave basis set was 450 eV. The Brillouin zones of the 2×2 and  $\sqrt{3}\times\sqrt{3}$  (111) supercells were sampled with 6×6×1 Monkhorst-Pack grids,<sup>15</sup> which guaranteed convergence of binding energies within a range of 0.05 eV. The Fermi level was smeared with the Methfessel-Paxton approach<sup>16</sup> with an electronic temperature of 0.2 eV, and all energies were extrapolated to T = 0 K. The relaxations of the atoms were carried out with the quasi-Newton minimization scheme, until the maximum force on any atom was below 0.05 eV Å<sup>-1</sup>. Ionic cores were described by Projector Augmented Wave (PAW) potentials.<sup>17</sup> All energies reported here are free energies calculated from DFT, vibrational analyses to estimate zero-point energies and vibrational frequencies, and thermodynamic tables to estimate entropy corrections to gas-phase species, through the expression:  $\Delta G = \Delta E_{DFT} + \Delta ZPE - T\Delta S$ , as described elsewhere.<sup>18,19</sup> Besides, we took into account the contribution of vibrational entropies to the free energies of oxygenated adsorbates and lattice species. The DFT energies of adsorption of \*O, \*OH, and \*OOH ( $\Delta G_O$ ,  $\Delta G_{OH}$ , and  $\Delta G_{OOH}$ ), were calculated with respect to hydrogen and water, as shown in Reactions (1) to (3) and expressed mathematically in equation (4) to (6):



$$\Delta G_O = G_{*O} + G_{H_2} - G_* - G_{H_2O} \quad (4)$$

$$\Delta G_{OH} = G_{*OH} + 1/2 G_{H_2} - G_* - G_{H_2O} \quad (5)$$

$$\Delta G_{OOH} = G_{*OOH} + 3/2 G_{H_2} - G_* - 2G_{H_2O} \quad (6)$$

where \* stands for an adsorption site on the electrode. Note that these definitions capitalize on the equilibrium between protons, electrons and hydrogen gas in aqueous media ( $1/2 H_2 \rightarrow H^+ + e^-$ ) to avoid two well-known problems: first the calculation of solvated protons, the appropriate energies of which cannot be obtained within the standard DFT formalism; and second the use of the value of the absolute standard hydrogen electrode potential, a number with large uncertainty in the literature, with reported values ranging from 4.28 to 4.85 V (See references 18,20,21 and references therein).

The energies of different surface states are computed with increasing potential on the Reversible Hydrogen Electrode (RHE) scale by thin-layer oxides. In these calculations, oxygenated species (\*O, \*OH, \*OOH) occupy substitutional positions in the top layer of Au (111) lattices and distort the normal configuration of the atoms due to the differences in Au-Au and Au-O distances.

## 2.3. Results

### 2.3.1. Experimental results

Figure 1a shows the linear-sweep voltammetry ( $0.001 \text{ V s}^{-1}$ ) of water oxidation on a polycrystalline gold electrode in 1.0 M  $\text{HClO}_4$ , together with an enlargement of the onset of the anodic current, and Figure 1b shows the cyclic voltammogram of the gold electrode recorded between 0 and 1.8 V vs. RHE. These results show that the formation of gold surface (hydr)oxides starts at *ca.* 1.3 V and that the onset of continuous anodic current is at *ca.* 1.9 V vs. RHE. *In situ* SERS experiments during electrochemical water oxidation in aqueous solution on gold surfaces in 1.0 M  $\text{HClO}_4$  were performed in order to confirm the signal around  $820 \text{ cm}^{-1}$  observed by Yeo et al.<sup>9</sup> The potential-dependent vibrational spectra acquired in normal water under steady state conditions are shown in Figure 1c. The spectra exhibit the characteristic features previously reported.<sup>22</sup> The sharp signal at *ca.*  $935 \text{ cm}^{-1}$  corresponds to the stretching vibration of Cl-O due to perchlorate anions. The perchlorate signal does not depend on the electrode potential, and only starts decreasing at very positive potentials at which the oxide layer is thick enough to affect the surface enhancement. Both

observations suggest that the observed perchlorate is in the double layer near the gold surface, but that it is not adsorbed. The broad signal centered around  $580\text{ cm}^{-1}$  is related to the Au-O vibration of the gold surface oxide, in agreement with earlier observations by Desilvestro and Weaver<sup>22</sup> and Yeo et al.<sup>9</sup> Remarkably, we also observe a shoulder on this broad band at *ca.*  $650\text{ cm}^{-1}$ , that has not been observed in previous works.

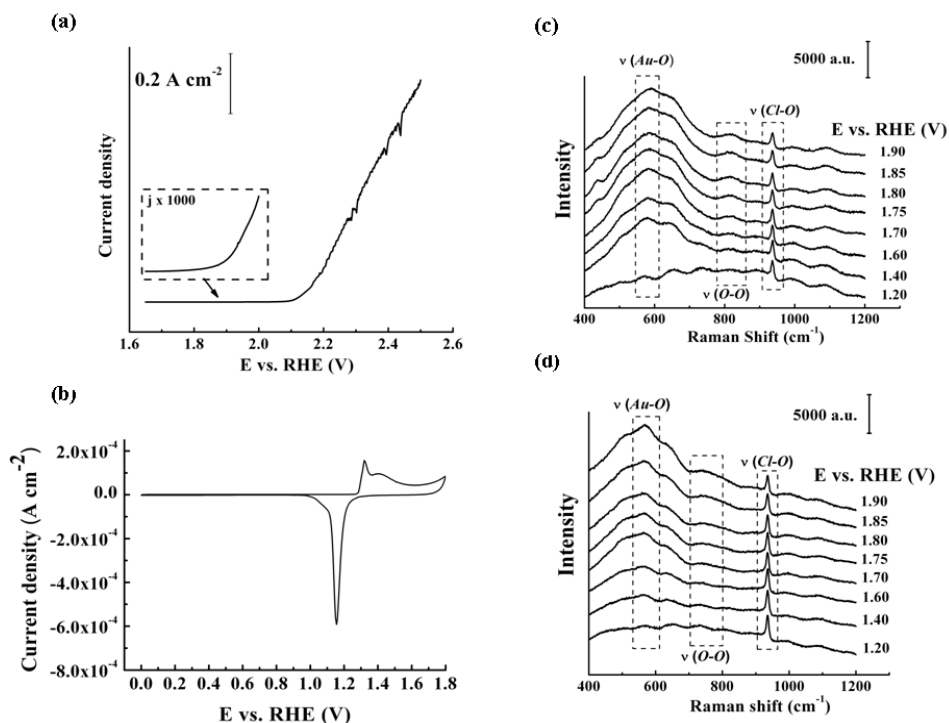


**Figure 1.** a) Linear sweep voltammety for oxygen evolution reaction on gold electrode at  $0.001\text{ V s}^{-1}$ . The current below  $2.0\text{ V}$ , multiplied by a factor of  $1000$ , is shown as inset in the voltammogram. b) Cyclic voltammety for gold electrode showing the “surface oxide” formation, acquired at  $0.05\text{ V s}^{-1}$ . c) SERS spectra for oxygen evolution acquired at constant potential in  $^{16}\text{O}$  water, d) Same as b) but experiments performed in  $^{18}\text{O}$  water. The experiments were performed in aqueous solution of  $\text{pH} = 1$ .

According to Desilvestro and Weaver,  $^{22}\text{Au}(\text{OH})_3$  and  $\text{Au}_2\text{O}_3$  exhibit Raman bands at 650 and 635  $\text{cm}^{-1}$ , respectively. As Desilvestro and Weaver have noted, the broadness of the gold-oxide band suggests “a wide multiplicity of surface oxide structures formed simultaneously, possibly involving different coordination geometries and hydration states of the gold atoms.” In alkaline media, Desilvestro and Weaver observed the stretching frequency of Au-OH at around 425  $\text{cm}^{-1}$ , shifting to higher frequencies with more positive potential, indicating the formation of gold surface oxides.

In agreement with Yeo et al.,<sup>9</sup> we also observe a signal around 810  $\text{cm}^{-1}$  that starts appearing at potentials positive of 1.4 V, and that was attributed to an OOH species adsorbed on the gold (oxide). From a comparison to the voltammetric data in Figure 1a, we conclude that this vibrational signal is observed at least 0.4 V less positive than the onset of water oxidation. Yeo et al. state that “it is not surprising that OOH species are observed before visible commencement of  $\text{O}_2$  gas evolution because the elementary steps of the OER process occur sequentially over a range of potentials starting from 1.1 V (vs. Ag/AgCl)”. However, we do consider this surprising. DFT calculations of OOH adsorption on gold, gold oxides, and many other materials suggest that this species is highly unstable,<sup>7,8,19</sup> and therefore should decompose into  $\text{O}_2$  rapidly. In the sequence of the elementary steps of the currently accepted OER mechanism, the OOH intermediate is the highest energy intermediate. Its spectroscopic observation over the potential range which essentially corresponds to the formation of the gold surface oxide (compare to the cyclic voltammetry in Figure 1b) is at least unexpected if not unlikely. In order to further elucidate the chemical identity of the species corresponding to this Raman band, spectroelectrochemical experiments were performed in  $\text{HClO}_4$  solutions made with  $^{18}\text{O}$  enriched (98%) water. Figure 1d shows the SERS spectra for water oxidation in  $^{18}\text{O}$  water. As expected, the signal corresponding to the perchlorate stretching does not shift when  $^{16}\text{O}$  water is replaced by  $^{18}\text{O}$  water. On the other hand, the signals corresponding to Au-O vibrations have shifted to lower frequencies due to the isotope effect. Table 1 compares the peak positions in  $^{16}\text{O}$  water, in  $^{18}\text{O}$  water and in deuterated  $^{16}\text{O}$  water, for three potentials. The band ascribed to the Au-O vibration near 580  $\text{cm}^{-1}$  exhibits a lowering close to the expected 5.7 % isotope

shift, but the signal around  $810\text{ cm}^{-1}$  exhibits a larger frequency shift than expected (*ca.* 10% vs. the expected 5.7%). However, we note that the position of the maximum of this broad peak is difficult to determine (as illustrated in Figure A1 in Appendix A), and moreover for the spectra in  $^{18}\text{O}$  water, the broad peak lies on the shoulder of the  $560\text{ cm}^{-1}$  feature, an effect that may artificially lower the actual frequency. Experiments were also performed in deuterium oxide ( $\text{D}_2\text{O}$ ). For the Au-O band a lowering in frequency is observed, but there was no significant shift in the O-OH signal compared to normal water (see Table 1, the corresponding spectra are shown in Figure A2 in Appendix A). Note that Yeo et al.<sup>9</sup> reported a shifting of that peak to higher frequencies when experiments were performed in deuterium oxide and suggested that to be due to isotopic effects. Although such a positive shift is opposite to the expected shift using the harmonic oscillator model, they attributed the small increase in frequency to the coupling between O-O and O-D modes. However, our results do not confirm this small shift.

**Table 1.** Vibrational frequencies for the Au-O and O-OH peaks as function of potential in pH 1 solution prepared respectively in  $^{16}\text{O}$ ,  $^{18}\text{O}$  water and  $\text{D}_2\text{O}$ .

E vs. RHE (V)	$\nu / \text{cm}^{-1}$					
	Au-O			O-OH		
	$^{16}\text{O}$ water	$^{18}\text{O}$ water	$\text{D}_2\text{O}$	$^{16}\text{O}$ water	$^{18}\text{O}$ water	$\text{D}_2\text{O}$
1.7	584	562	578	811	734	808
1.8	586	564	579	812	738	812
1.9	589	567	581	810	734	810

In order to probe the involvement of the gold surface oxide in the generation of molecular oxygen during OER, online electrochemical mass spectrometry (OLEMS) experiments were performed. Figure 2 shows the results for oxygen evolution from normal water, confirming that the anodic current is mirrored by the detection of oxygen in the mass

spectrometer. From the enlargement of the  $^{32}\text{O}_2$  signal, we conclude that oxygen evolution starts at *ca.* 2.0 V, and it is difficult to claim that oxygen is evolved below that potential. In a separate experiment, the gold electrode was oxidized in a two-electrode cell filled with  $^{18}\text{O}$  water at 2.0 V so as to generate an  $^{18}\text{O}$  enriched gold oxide on the gold.

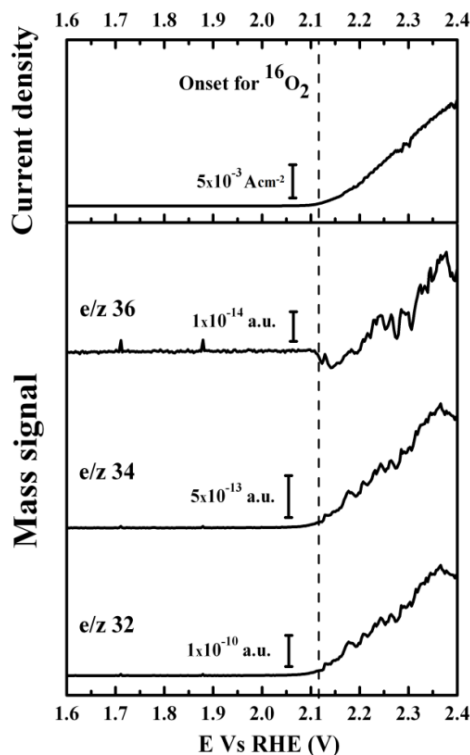


**Figure 2.** Linear sweep voltammetry for oxygen evolution reaction on a gold electrode in a 1 M  $\text{HClO}_4$  solution prepared with  $^{16}\text{O}$  water. b) OLEMS signals during oxygen evolution corresponding to different isotopes of dioxygen ( $^{16}\text{O}_2$ ,  $^{16}\text{O}^{18}\text{O}$  and  $^{18}\text{O}_2$ ) as a function of applied potential. Scans were made at  $0.001 \text{ V s}^{-1}$ .

Next, the thus generated gold oxide electrode was transferred to an  $^{16}\text{O}$  aqueous electrolyte. Figure 3a shows the resulting current-potential profile during the positive linear scan, alongside the signals recorded in the mass spectrometer corresponding to various

isotopes of dioxygen (namely  $^{16}\text{O}_2$ ,  $^{16}\text{O}^{18}\text{O}$  and  $^{18}\text{O}_2$  species) produced during oxygen evolution (figure 3b). In agreement with Figure 2b, no dioxygen is detected in the mass spectrometer at potentials lower than 2.0 V but as can be seen in figure 3b,  $^{18}\text{O}_2$  is the first oxygen product evolved from the gold oxide layer with no apparent increase in signal corresponding to  $^{16}\text{O}_2$ . This would indicate that a kind of oxide decomposition mechanism is operative, at least in the very early stages of the oxygen evolution reaction. Previous similar online mass spectrometry experiments conducted with  $\text{RuO}_2$  and  $\text{IrO}_2$  electrodes in (partially) isotopically labeled water has indicated an oxygen exchange (or Mars-Van Krevelen-type) mechanism, but has not provided evidence for the oxide decomposition mechanism (or disproportionation mechanism, see Discussion) suggested by Figure 3.<sup>23-25</sup>

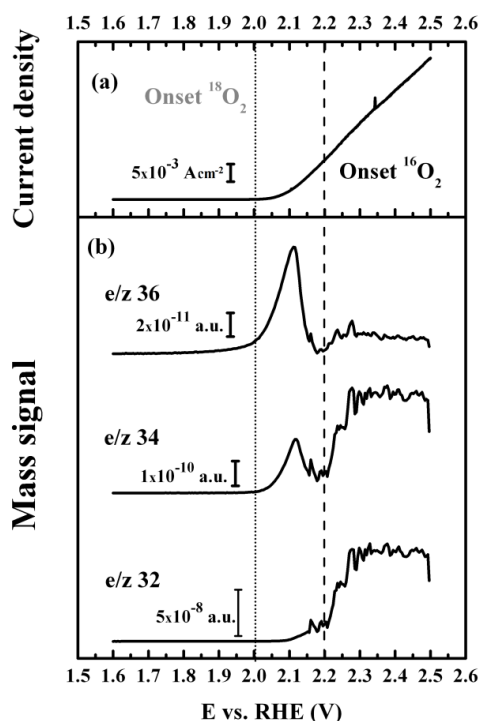


**Figure 3.** Linear sweep voltammetry for oxygen evolution reaction on  $^{18}\text{O}$  gold oxide performed in a 1 M  $\text{HClO}_4$  solution prepared with  $^{16}\text{O}$  water. b) OLEMS signals during oxygen evolution on the gold electrode corresponding to different isotopes of dioxygen ( $^{16}\text{O}_2$ ,  $^{16}\text{O}^{18}\text{O}$  and  $^{18}\text{O}_2$ ) as function of potential. Scans were made at  $0.001 \text{ V s}^{-1}$ .

Since it is to be expected that the nature of the oxide layer formed on gold depends on the gold surface structure, we have determined the oxygen-evolving activities of three low-index gold single-crystal surfaces. Figure 4 shows the cyclic voltammetry of the three electrodes for  $0 < E < 1.75 \text{ V}$ , in good agreement with the ones reported in the literature,<sup>26,27</sup> and the Tafel plots of the same electrodes for  $1.85 < E < 2.16 \text{ V}$ . The Tafel plots clearly show two different slopes, 112-163 mV/dec for  $E < 2.0 \text{ V}$ , for which we do not observe oxygen in the mass spectrometer, and 42-46 mV/dec for  $E > 2.0 \text{ V}$ , corresponding to the potential region of oxygen evolution. The latter Tafel slope agrees well with the values reported many decades ago.<sup>28</sup> Interestingly, there is a clear structure sensitivity, the Au(110) surface being the most active surface, and the Au(100) surface being the least active, although we realize that under surface oxide forming and oxygen-evolving conditions, these surfaces no longer exhibit their nominal structure.

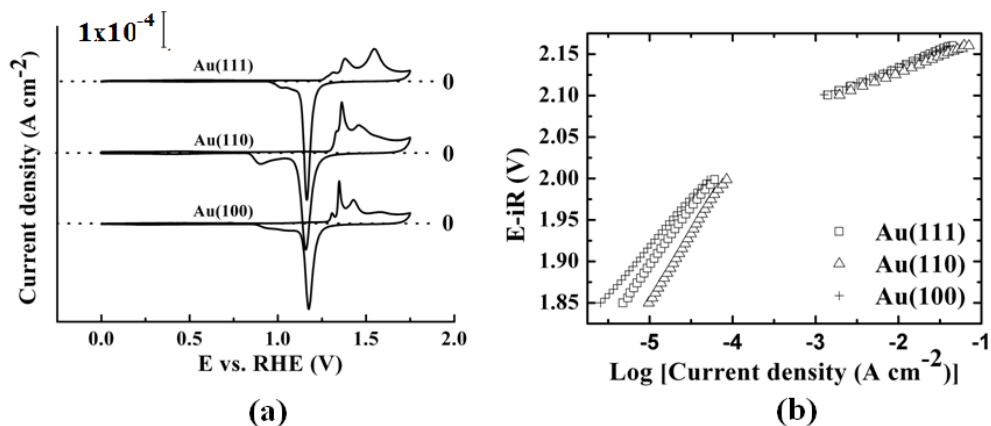


**Figure 4.** a) Cyclic voltammetry for the three low-index gold single crystals in 1 M  $\text{HClO}_4$  solution prepared with  $^{16}\text{O}$  water, Scan rate:  $0.05 \text{ V s}^{-1}$ . b) Tafel plot obtained from a linear sweep voltammetry to oxygen evolution potentials with the three low-index gold single crystals. Scan rate:  $0.001 \text{ V s}^{-1}$ .

Finally, in Figure 5 we plot the charge measured in the reduction of gold oxide between 0.8 and 1.3 V as a function of the positive limit potential in a previous linear-sweep voltammogram. The charge is expressed in monolayer equivalents, where one monolayer is  $390 \mu\text{C}\cdot\text{cm}^{-2}$ .<sup>29</sup> This plot is very similar to others available in the literature<sup>30</sup>, and is included here to illustrate that there appears to be a leveling off in oxide-layer growth between 1.5 and 2 V, and that oxygen evolution starts, at *ca.* 2.0 V, after the completion of an oxide layer of 3 ML equivalents.

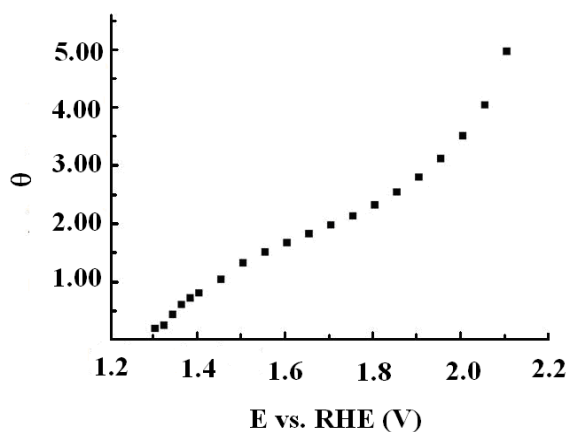
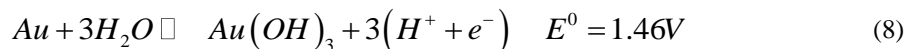
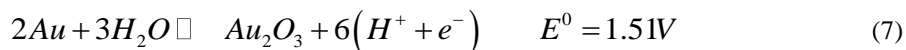


**Figure 5.** Oxygen coverage on a gold electrode as a function of positive potential limit during anodic polarization.

### 2.3.2. Brief summary of literature on the surface oxidation of gold

Before we discuss the computational results, it is useful to briefly summarize some of the most relevant experimental results from the extensive literature of electrochemical gold surface oxide formation. First of all, gold is the only metal that is thermodynamically stable at potentials above the potential of the water oxidation. Pourbaix diagrams of gold typically consider only two stable forms of gold oxide or hydroxide, *i.e.* gold(III) oxide and hydroxide<sup>31,32</sup>:



Note that these two reactions imply:



In fact, hydrous  $Au_2O_3$  is often considered equivalent to gold(III) hydroxide.  $Au(OH)_3$  is a planar compound, not soluble in water. Gold oxides with oxidation states other than Au(III) are unstable and extremely rare<sup>33</sup>. Previous claims of  $Au_2O$  and  $AuO$  in fact turned out to be mixtures of Au and  $Au_2O_3$ .<sup>34</sup>

Several authors have attempted to characterize the oxidation state of gold oxides grown electrochemically. Using *ex situ* X-ray Photoelectron Spectroscopy (XPS), Peuckert et al.<sup>34</sup> studied thin oxide layers on Au(100), and Juodkazis et al.<sup>35</sup> studied thin oxide layers on polycrystalline gold, both in sulfuric acid electrolyte. Au(III) was the only Au oxidation state observed. According to Peuckert et al.,<sup>34</sup> initially a  $Au(OH)_3$  layer is formed, and from 2.0 V the layer is further deprotonated or dehydrated to gold oxyhydroxide  $AuOOH$  (“meta gold acid”), which is supposed to initiate more rapid film growth. Near 2.0 V, the  $Au(OH)_3$  is suggested to consist of “beyond two”<sup>34</sup> or “three”<sup>35</sup> monolayers. Thermal decomposition of electrochemically prepared  $AuOOH$  does not lead to anhydrous  $Au_2O_3$  but to decomposition into a mixture of Au and  $Au_2O_3$  with the concomitant formation of molecular oxygen  $O_2$ .<sup>34</sup> Interestingly, Peuckert et al. find evidence for molecular oxygen “trapped” or “dissolved” in thick oxide layers, the nature of which has remained unclear. A similar kind of molecular oxygen or peroxide occluded in intergrain voids of  $Au_2O_3$  grown in the gas phase was observed by exposing polycrystalline gold to activated oxygen.<sup>36</sup> Moreover, *in situ* EXAFS studies by Weiher<sup>37</sup> detected only Au(III) in electrochemically grown gold oxide layers, and concluded that electrochemical  $Au_2O_3$  is highly disordered.

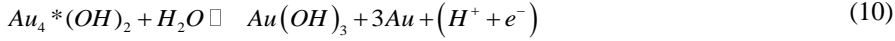
Detailed electrochemical studies of oxide layers grown on (single-crystalline) gold electrodes have shown that the initial adsorption of OH to the gold surface at *ca.* 1.3 V is reversible, but is rapidly followed by further oxidation including place exchange between gold and oxygen atoms, leading to a quasi three-dimensional hydroxy-oxide film.<sup>27,38,39</sup> According to Conway, at 1.6 V AuOH is further oxidized to a AuO surface film. From quartz crystal microbalance and ellipsometry measurements, Xia and Birss<sup>40</sup> have concluded that the thin (“compact”) oxide layer consists of AuO below 1.5 V, and of a mixture of AuO and Au<sub>2</sub>O<sub>3</sub> above 1.5 V. Up to three monolayers of this thin Au<sub>2</sub>O<sub>3</sub> ( $\alpha$ -oxide) layer can be formed before a thicker oxide ( $\beta$ -oxide) film forms.

### 2.3.3. Computational results

The foregoing brief summary of the interpretation of the experimental results suggests that although surface oxide formation on gold electrodes has been extensively studied, there is currently no universally accepted interpretation for all the observed features, especially those observed at higher potentials. Therefore, we have undertaken a DFT-based computational study of the surface thermodynamics of electrochemical gold, which suggests that the Au(111) surface experiences, at least, the five changes listed below as the potential is successively increased, and as illustrated in Figure 6 (analogous analyses can in principle be made for other surface facets). It is important to remark at this point that PBE, the xc-functional used in our calculations, typically overbinds adsorbates with respect to the experimentally observed values<sup>41</sup> and hence we expect to find deviations on the order of  $\sim 0.2$  V in the computed values when compared to the experiments presented here and in references.<sup>27,34,38</sup>

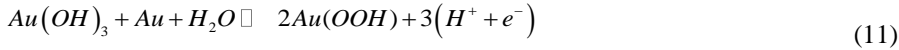
1. \*OH adsorption: At 1.05 V vs. RHE the adsorption of \*OH becomes thermodynamically favorable on the Au(111) surface. The reaction that describes the process is given in equation (2). The quoted potential corresponds to a \*OH coverage of 1/3 ML, modeled in a  $\sqrt{3}\times\sqrt{3}$  (111) supercell. In this case we added a correction of -0.55 eV to the free energy accounting for the solvation of the \*OH groups, similar to that recommended by Tripkovic et al for Pt(111) under ORR conditions.<sup>42</sup>

2. Gold(III) hydroxide formation: At 1.17 V vs. RHE the oxidation of the surface is such that a thin layer of Au(OH)<sub>3</sub> is formed at the surface of the electrode. The reaction that describes the process is given in equation (10).



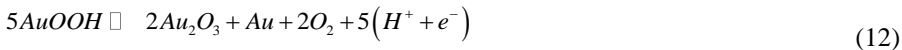
where Au<sub>4</sub>\* (OH)<sub>2</sub> denotes a 2×2 (111) supercell of Au with 2 \*OH groups adsorbed on it (*i.e.* the coverage is ½ ML). Moreover, the Au atoms that are freed during this reaction and the following reactions are supposed to be incorporated into the bulk or to accumulate in Au islands at the surface, which will in turn be oxidized. Therefore, we consider it likely that this reaction would be responsible for the onset of Au(111) surface roughening, as it involves the formation of a monolayer of surface hydroxide.

3. AuOOH formation: at 1.28 V vs. RHE the hydroxide (Au(OH)<sub>3</sub>) turns into an oxyhydroxide. The reaction that describes this process is given in equation (11).



It is to be noted here that in both oxyhydroxide and hydroxide the formal gold oxidation state is Au<sup>3+</sup> and, therefore, they differ mainly in their degree of hydration. We also calculated AuOOH in the hydroperoxide structure; however this compound is less stable than its oxyhydroxide isomer by *ca.* 0.75 eV/OOH.

4. Oxide Formation: at 1.54 V vs. RHE the oxyhydroxide is further dehydrated to Au<sub>2</sub>O<sub>3</sub> (modeled in a 5×2 (111) supercell). We chose Au<sub>2</sub>O<sub>3</sub> in our model, as several studies referred to above have concluded that the Au(III) oxidation state is dominant, but several other oxides can in principle be formed, including AuO<sub>2</sub>, as reported by Pourbaix,<sup>32</sup> as well as other non-stoichiometric oxides. The reaction that describes the oxidation process is given in equation (12).



5. Catalytic Oxygen Evolution: at 1.95 V vs. RHE the oxide surface starts the actual catalysis of the oxygen evolution reaction (OER). The overall process is given by the reaction:  $2H_2O \rightarrow O_2 + 4(H^+ + e^-)$ . The onset potential is estimated from the potential-determining step (PDS), *i.e.* the step in the mechanism that corresponds to the thermodynamically least favorable step in the mechanism and that thereby determines the minimum value of the onset potential of the reaction. According to the model by Man et al.<sup>19</sup>, which is based on values of the adsorption energies of \*O, \*OH, and \*OOH, the PDS in our case is the following:



On the other hand, the predicted OER onset potentials for Au(OH)<sub>3</sub> and AuOOH are 2.22 V and 2.39 V, respectively. Regardless of the active phase generating oxygen, oxidized surfaces containing Au<sup>3+</sup> are expected to have large overpotentials for OER and to be located on the leg of the volcano curve corresponding to weak oxygen adsorption, as proposed by Man et al.<sup>19</sup>

We note at this point that the conclusions of the experimental works by Conway et al.<sup>38</sup> with Au(111) electrodes in 0.01M HClO<sub>4</sub> are rather similar to our proposal in Figure 6. They suggest that a water adlayer will turn into an \*OH adlayer on Au(111) electrodes at potentials around 1.2 V vs. RHE. Moreover, the process will turn into a surface oxidation leading to Au(OH)<sub>3</sub> at potentials between 1.2 and 1.35 V vs. RHE. Besides, at potentials over 1.55 V vs. RHE they proposed that the surface will be composed of AuOOH as an oxyhydroxide capable of evolving oxygen catalytically. We conclude at this point that the (111) surface undergoes several stoichiometric and structural changes as the potential is anodically raised before it starts evolving oxygen catalytically, and that the hydration of the surface compounds decreases as the potential is increased. Also note from Figure 6 that the configuration of the Au atoms in the Au(111) surface changes as the gold(III) hydroxide phase is formed, suggesting that, as mentioned, at this point an electrochemical surface roughening could be introduced.

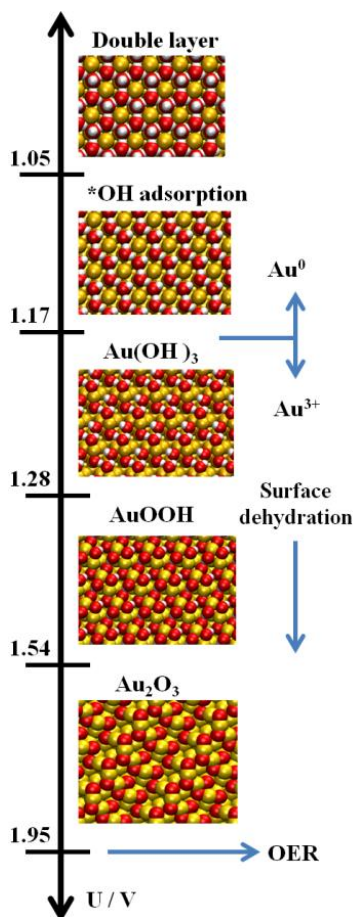


**Figure 6.** Schematics of the different stable surface states with increasing potential on a Au(111) electrode, as estimated from the DFT calculations. The double layer region is followed by \*OH adsorption at 1.05 V vs. RHE, gold(III) hydroxide formation at 1.17 V, initial dehydration to form an oxyhydroxide 1.28 V, further dehydration to form a surface oxide at 1.54 V, and catalytic oxygen evolution at 1.95 V.

A second objective of our DFT calculations is to perform a vibrational analysis of possible intermediates, primarily aimed at the SERS signal at  $810 \pm 50 \text{ cm}^{-1}$ . From a theoretical point of view, one can support the experimental claim that the signal corresponds to a stretching of O-O bonds at the surface on the basis of the vibrational frequencies of \*O, \*O<sub>2</sub>, \*OH, and \*OOH on Au(111) and (211), and the values are shown

in Table 2. Note that the (211) facets are stepped surfaces with short (111) terraces and (100) steps.

**Table 2.** Selected vibrational frequencies of various species on their most stable adsorption sites on Au(111) and (211). In general, the vibrational frequencies decrease when the coordination number of the metal site is reduced. In all cases, only the closest frequencies to  $810 \pm 50 \text{ cm}^{-1}$  are provided.

Species	$\nu / \text{cm}^{-1}$	
	111	211
*O	361	449
*O <sub>2</sub>	1278	1064
*OH	808	729
*OOH	860	823

From Table 2 we observe that, except for the vibrational frequencies of \*O, those of the other adsorbates decrease upon reduction of the coordination number of the metal site to which the adsorbate is bound: the coordination number of the metal atoms at (111) surfaces is 9, whereas it is 7 at the step edge of (211) surfaces. Since the (111) is the most closed-packed surface of all fcc metal surfaces, its vibrational frequencies can be regarded as an upper bound for the Raman peaks, whereas those at the steps may be taken as a lower bound. Based on this approximation, only \*OOH adsorbates fall in the appropriate range of frequencies found in the experiments ( $810 \pm 50 \text{ cm}^{-1}$ ). Moreover, a glimpse at O-O stretching frequencies of some related gas-phase compounds such as O<sub>2</sub> (DFT:  $1549 \text{ cm}^{-1}$ , reported:  $1580 \text{ cm}^{-1}$ <sup>43</sup>), H<sub>2</sub>O<sub>2</sub> (DFT:  $914 \text{ cm}^{-1}$ , reported:  $864 \text{ cm}^{-1}$ <sup>43</sup>), Au<sub>2</sub>O<sub>2</sub> (DFT:  $991 \text{ cm}^{-1}$ ), and AuOOH (DFT:  $872 \text{ cm}^{-1}$ ), reveals that the O-O bond in question is single and that the oxygen atoms should be coordinated to Au and H atoms.

In order to discard that \*OH groups could be responsible for the observed Raman signal, we also calculated the vibrational frequencies of \*OH and \*OOH on several Au facets, and the results are shown in Table 3. The arithmetic averages of the frequencies ( $754 \pm 43 \text{ cm}^{-1}$  and  $824 \pm 26 \text{ cm}^{-1}$ ) serve as a rough estimate of the expected centers of the peaks and confirm that only O-O stretching is expected at the experimental range of frequencies ( $810 \pm 50 \text{ cm}^{-1}$ ).

**Table 3.** Vibrational frequencies of \*OH and \*OOH adsorbates on various Au surfaces. The coordination numbers (CN) are provided in each case to facilitate the observation of the trends. In both cases, a decrease in CN is well correlated with a decrease in the vibrational frequencies.

facet / adsorbates	$\nu / \text{cm}^{-1}$	
	*OOH	*OH
111 (CN = 9)	860	808
100 (CN = 8)	801	767
211 (CN = 7)	823	729
110 (CN = 6)	810	712
Average	824	754
Standard deviation	26	43

Moreover, we calculated the vibrational frequencies of  $\text{Au}(\text{OH})_3$  ( $928 \text{ cm}^{-1}$ ),  $\text{AuOOH}$  ( $945 \text{ cm}^{-1}$ ) and  $\text{Au}_2\text{O}_3$  ( $600 \text{ cm}^{-1}$ ) to verify that \*OH and \*O groups belonging to thin-layer structures in oxidized Au(111) do not exhibit any vibrations in the region around  $810 \pm 50 \text{ cm}^{-1}$ . It is also noteworthy that the expected frequency of  $810 \pm 50 \text{ cm}^{-1}$  does not appear when \*OOH is adsorbed on oxidized Au atoms as shown in Table 4, where one can see that the O-O stretching frequencies of \*OOH adsorbed on  $\text{Au}(\text{OH})_3$ ,  $\text{AuOOH}$  and  $\text{Au}_2\text{O}_3$  are over  $930 \text{ cm}^{-1}$ . On the other hand, those of rough Au(111) (simulated as a  $2 \times 2$

(111) unit cell with a missing row of Au atoms in the top layer) and pristine Au(111) are near  $850\text{ cm}^{-1}$ .

**Table 4.** O-O stretching frequencies of \*OOH adsorbates on various surface compounds of Au. When Au atoms are oxidized, the frequency of the O-O stretching increases, and as seen before in Table 3, \*OOH adsorbed on under-coordinated Au atoms have lower O-O frequencies.

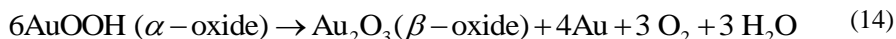
surface species	$\nu_{\text{O-O}} / \text{cm}^{-1}$
Au(111)	860
Au(111) (rough)	840
Au(OH) <sub>3</sub>	976
AuOOH	996
Au <sub>2</sub> O <sub>3</sub>	939

The observations in Tables 2 to 4 suggest that the frequency around  $810 \pm 50\text{ cm}^{-1}$  belongs to an O-O stretching from oxygen atoms bound on one side to a gold atom and on the other to a hydrogen, and that those Au atoms are not oxidized and have low coordination numbers. This in turn suggests that the formation of Au(OH)<sub>3</sub> and the other subsequent oxidation products should be accompanied by a noticeable roughening of the surface and by disproportion reactions that create Au islands. These observations are in agreement with the STM results of Schneeweiss and Kolb<sup>39</sup> and with the general mechanism of gold oxide formation proposed by Angerstein-Kozłowska and Conway.<sup>27,38</sup>

## 2.4. Discussion

The results presented in the previous sections are strongly suggestive of a mechanism for oxygen evolution that is considerably different from previous mechanisms suggested in the literature.<sup>6-8</sup> The combined electrochemistry and online mass spectrometry experiments

suggest that the first oxygen evolves at the transition from the  $\alpha$ - to the  $\beta$ -oxide, after three monolayers of  $\text{Au}(\text{OH})_3$  or hydrous  $\text{Au}_2\text{O}_3$  oxide have been formed. Our OLEMS results show that the first oxygen that evolves consists completely of oxygen atoms from the oxide. This would be consistent with Peuckert's<sup>33</sup> suggestion that the  $\text{AuOOH}$  that starts to be formed at 2.0 V is not stable but decomposes according to the overall reaction:



This  $\text{Au}_2\text{O}_3$  is not exactly the same as that formed below 2.0 V as it is used to build up the thicker  $\beta$ -oxide<sup>39</sup>. As mentioned in section 2.3.2, below 2.0 V a hydrous form of  $\text{Au}_2\text{O}_3$  exists on the surface. Equation (15) is essentially a dehydration reaction accompanied by oxygen evolution, due to lack of hydrogen. The Au in equation (16) will be either oxidized very rapidly, or it will make part of the underlying Au substrate, as the gold oxide layer is very thin. In fact, equation (17) can also be considered a disproportionation reaction, in which a lower valence hydrous metal oxide disproportionates into a higher valence metal oxide and the metal, under the release of water and dioxygen. The oxidized gold surface is very rough, covered by non-ordered oxide, and the roughening process seems to be initiated by the formation of the gold(III) hydroxide. The SERS and DFT results presented here (and those by Yeo *et al.*<sup>9</sup>) would indicate that  $\text{O}_2$  does not form all of a sudden, but a precursor is existent already within the oxide, probably somehow related to highly non-ordered structure. The idea of such a peroxidic species existing within the oxide layer is in fact not new.<sup>33, 35</sup> This species is released as the more stable molecular oxygen as soon as the transition to the  $\beta$ -oxide occurs.

In brief, the key ingredients of this new model for oxygen evolution are: (i) peroxide or O-O species already exists within the thin 3D non-ordered oxide, (ii) the first oxygen that is released evolves from this species (which is not a pure surface species) as a result of a change in hydration state of the oxide film, by oxide decomposition or oxide disproportionation, at least initially at the onset potential. Of course, after this initial oxygen release, or at higher potentials, other mechanisms may also be involved, more similar to the

oxygen exchange mechanisms concluded from earlier online mass spectrometry measurements.<sup>23-25</sup>

## 2.5. Conclusions

In search for a more atomic-level understanding of the mechanism(s) through which water splits electrochemically, we have revisited the electrocatalysis of O<sub>2</sub> evolution on gold electrodes through a variety of experimental techniques and DFT calculations. *In situ* SERS measurements showed the appearance of a peak located at 810 cm<sup>-1</sup> at potentials over 1.4 V vs. RHE, while the OER only starts at potentials around 2.0 V vs. RHE. Isotopic labeling and DFT calculations help assigning this peak to an O-O stretching of \*OOH species presumably incorporated into a highly disordered surface oxide. DFT calculations confirm that the oxidation of the electrode as the potential is successively increased should be accompanied by a significant roughening and dehydration of the surface. OLEMS measurements show the existence of an oxide-layer depletion mechanism at early stages (~2.0 V vs. RHE) of the OER. This initial evolution of oxygen consisting of two oxygen atoms from the surface oxide suggests an oxide decomposition or oxide disproportionation step. At higher electrode potentials (~2.05 V vs. RHE), O<sub>2</sub> is evolved from a combination of oxygen atoms from the surface oxide and water. These results show that electrocatalytic surfaces for oxygen evolution may undergo dynamic changes during the advance of the reactions, that several pathways are possible for a given reaction at different potentials, and that, most significantly, the oxygen evolved on a gold electrode at the onset potential appears to be the product of an oxide decomposition step.

## 2.6. Acknowledgments

This research is financed in part by the BioSolar Cells open innovation consortium, supported by the Dutch Ministry of Economic Affairs, Agriculture and Innovation. Financial support from the Netherlands Organization for Scientific Research (NWO) and the National Research School Catalysis (NRSC) is gratefully acknowledged. We also acknowledge the Stichting Nationale Computerfaciliteiten (National Computing

Facilities Foundation, NCF) for the use of their supercomputer facilities, with financial support from the NWO. Dr. F. Calle-Vallejo is kindly acknowledged for his computational contributions to the project. Special thanks to C. de Munck for his assistance with the OLEMS experiments.

## REFERENCES

- (1) de Levie, R. *J. Electroanal. Chem.* **1999**, *476*, 92.
- (2) Paets van Troostwijk, A.; Deiman, J. R. *Obs. Phys.* **1789**, *35*, 369.
- (3) Dau, H.; Limberg, C.; Reier, T.; Risch, M.; Roggan, S.; Strasser, P. *Chemcatchem* **2010**, *2*, 724.
- (4) Lewis, N. S.; Nocera, D. G. *Proc. Natl. Acad. Sci. U. S. A.* **2006**, *103*, 15729.
- (5) Matsumoto, Y.; Sato, E. *Materials Chemistry and Physics* **1986**, *14*, 397.
- (6) Trasatti, S. *J. Electroanal. Chem.* **1980**, *111*, 125.
- (7) Rossmeisl, J.; Logadottir, A.; Norskov, J. K. *Chem. Phys.* **2005**, *319*, 178.
- (8) Rossmeisl, J.; Qu, Z. W.; Zhu, H.; Kroes, G. J.; Norskov, J. K. *J. Electroanal. Chem.* **2007**, *607*, 83.
- (9) Yeo, B. S.; Klaus, S. L.; Ross, P. N.; Mathies, R. A.; Bell, A. T. *ChemPhysChem* **2010**, *11*, 1854.
- (10) Lai, S. C. S.; Kleyn, S. E. F.; Rosca, V.; Koper, M. T. M. *Journal of Physical Chemistry C* **2008**, *112*, 19080.
- (11) Gao, P.; Gosztola, D.; Leung, L. W. H.; Weaver, M. J. *J. Electroanal. Chem.* **1987**, *233*, 211.
- (12) Wonders, A. H.; Housmans, T. H. M.; Rosca, V.; Koper, M. T. M. *J Appl Electrochem* **2006**, *36*, 1215.
- (13) Kresse, G.; Furthmuller, J. *Phys. Rev. B* **1996**, *54*, 11169.
- (14) Perdew, J. P.; Burke, K.; Ernzerhof, M. *Phys. Rev. Lett.* **1996**, *77*, 3865.
- (15) Monkhorst, H. J.; Pack, J. D. *Phys. Rev. B* **1976**, *13*, 5188.
- (16) Methfessel, M.; Paxton, A. T. *Physical Review B* **1989**, *40*, 3616.
- (17) Kresse, G.; Joubert, D. *Phys. Rev. B* **1999**, *59*, 1758.

- (18) Nørskov, J. K.; Rossmeisl, J.; Logadottir, A.; Lindqvist, L.; Kitchin, J. R.; Bligaard, T.; Jónsson, H. *The Journal of Physical Chemistry B* **2004**, *108*, 17886.
- (19) Man, I. C.; Su, H.-Y.; Calle-Vallejo, F.; Hansen, H. A.; Martinez, J. I.; Inoglu, N. G.; Kitchin, J.; Jaramillo, T. F.; Nørskov, J. K.; Rossmeisl, J. *Chemcatchem* **2011**, *3*, 1159.
- (20) Tripkovic, V.; Bjorketun, M. E.; Skulason, E.; Rossmeisl, J. *Phys. Rev. B* **2011**, *84*.
- (21) Trasatti, S. *Pure Appl. Chem.* **1986**, *58*, 955.
- (22) Desilvestro, J.; Weaver, M. J. *Journal of Electroanalytical Chemistry and Interfacial Electrochemistry* **1986**, *209*, 377.
- (23) Wohlfahrt-Mehrens, M.; Heitbaum, J. *Journal of Electroanalytical Chemistry and Interfacial Electrochemistry* **1987**, *237*, 251.
- (24) Fierro, S. p.; Nagel, T.; Baltruschat, H.; Comminellis, C. *Electrochem. Commun.* **2007**, *9*, 1969.
- (25) Macounova, K.; Makarova, M.; Krtil, P. *Electrochem. Commun.* **2009**, *11*, 1865.
- (26) Conway, B. E. *Prog. Surf. Sci.* **1995**, *49*, 331.
- (27) Angersteinkozłowska, H.; Conway, B. E.; Hamelin, A.; Stoicoviciu, L. *Electrochimica Acta* **1986**, *31*, 1051.
- (28) Barnartt, S. J. *Electrochem. Soc.* **1959**, *106*, 991.
- (29) Trasatti, S.; Petrii, O. A. *Journal of Electroanalytical Chemistry* **1992**, *327*, 353.
- (30) Laitinen, H. A.; Chao, M. S. *J. Electrochem. Soc.* **1961**, *108*, 726.
- (31) Nicol, M. *Gold Bulletin* **1980**, *13*, 46.
- (32) Pourbaix, M. *Atlas of Electrochemical Equilibria in Aqueous Solutions*; Second English ed.; National Association of Corrosion Engineers: Houston, Texas, 1974.
- (33) Puddephatt, R. *The Chemistry of Gold*; Elsevier: New York, 1978.
- (34) Peuckert, M.; Coenen, F. P.; Bonzel, H. P. *Surf. Sci.* **1984**, *141*, 515.
- (35) Juodkazis, K.; Juodkazyte, J.; Jasulaitiene, V.; Lukinskas, A.; Sebek, B. *Electrochem. Commun.* **2000**, *2*, 503.
- (36) Stadnichenko, A. I.; Koshcheev, S. V.; Boronin, A. I. *Moscow University Chemistry Bulletin* **2007**, *62*, 343.
- (37) Weiher, N., Freie Universitaet, 2003.

- (38) Angersteinkozłowska, H.; Conway, B. E.; Hamelin, A.; Stoicoviciu, L. *Journal of Electroanalytical Chemistry* **1987**, 228, 429.
- (39) Schneeweiss, M. A.; Kolb, D. M. *Solid State Ionics* **1997**, 94, 171.
- (40) Xia, S. J.; Birss, V. I. *J. Electroanal. Chem.* **2001**, 500, 562.
- (41) Hammer, B.; Hansen, L. B.; Nørskov, J. K. *Phys. Rev. B* **1999**, 59, 7413.
- (42) Tripkovic, V.; Skulason, E.; Siahrostami, S.; Nørskov, J. K.; Rossmeisl, J. *Electrochim. Acta* **2010**, 55, 7975.
- (43) Nakamoto, K. *Infrared and Raman spectra of Inorganic and Coordination Compounds*; 4th ed.; John Wiley & Sons: Milwaukee, 1986.